

Cite this: *Chem. Sci.*, 2024, 15, 3165

All publication charges for this article have been paid for by the Royal Society of Chemistry

Single electron reduction of NHC–CO₂–borane compounds†

Agustín Morales,^{ab} Caroline Gonçalves,^a Alix Sournia-Saquet,^a Laure Vendier,^a Agustí Lledós,^{id}*^b Olivier Baslé,^{id}*^a and Sébastien Bontemps,^{id}*^a

The carbon dioxide radical anion [CO₂^{•-}] is a highly reactive species of fundamental and synthetic interest. However, the direct one-electron reduction of CO₂ to generate [CO₂^{•-}] occurs at very negative reduction potentials, which is often a limiting factor for applications. Here, we show that NHC–CO₂–BR₃ species – generated from the Frustrated Lewis Pair (FLP)-type activation of CO₂ by N-heterocyclic carbenes (NHCs) and boranes (BR₃) – undergo single electron reduction at a less negative potential than free CO₂. A net gain of more than one volt was notably measured with a CAAC–CO₂–B(C₆F₅)₃ adduct, which was chemically reduced to afford [CAAC–CO₂–B(C₆F₅)₃^{•-}]. This room temperature stable radical anion was characterized by EPR spectroscopy and by single-crystal X-ray diffraction analysis. Of particular interest, DFT calculations showed that, thanks to the electron withdrawing properties of the Lewis acid, significant unpaired spin density is localised on the carbon atom of the CO₂ moiety. Finally, these species were shown to exhibit analogous reactivity to the carbon dioxide radical anion [CO₂^{•-}] toward DMPO. This work demonstrates the advantage provided by FLP systems in the generation and stabilization of [CO₂^{•-}]-like species.

Received 27th November 2023

Accepted 18th January 2024

DOI: 10.1039/d3sc06325a

rsc.li/chemical-science

Introduction

The carbon dioxide radical anion [CO₂^{•-}] is a very unstable molecule that was characterized from trapping experiments with 5,5-dimethyl-1-pyrroline *N*-oxide (DMPO) by EPR,¹ using pulse radiolysis with time-resolved IR detection in acetonitrile,² by IR (hydrated form,³ on surfaces⁴ or in Ne matrix⁵), and by mass spectrometry in the gas phase.⁶ As a classical distonic anion, the charge and radical sites of [CO₂^{•-}] are separated.⁷ Notably, the radical is located on a σ -type orbital centred on the carbon atom.⁶ This highly reactive molecule was exploited in diverse synthetic approaches to produce carboxylic acid-containing molecules through C–C bond formation,⁸ or as a powerful single electron reductant in challenging reductive processes.^{8a,r,9}

The use of alkali formate compounds [MHCO₂] has recently emerged as an efficient method to generate [CO₂^{•-}] by Hydrogen Atom Transfer (HAT) (Chart 1a).^{8o-t} As an alternative, the direct one-electron reduction of CO₂ has been employed to generate [CO₂^{•-}] in few synthetic transformations by photo-

electroreduction.^{8b-n} However, such reduction is energy demanding since it requires very negative reduction potentials (*e.g.* $E_{1/2} = -2.65$ V in DMF, -2.70 V in CH₃CN and -2.53 V in aqueous solution *vs.* Fc⁺⁰),^{8b,10} which limits practical applications (Chart 1a). In the context of using CO₂ as a sustainable source of carbon,¹¹ it is therefore appealing to seek CO₂ activation modes that would enable an easier one-electron reduction process to access [CO₂^{•-}]. With this in mind, we decided to investigate the single electron reduction of FLP (Frustrated Lewis Pair)-type activated CO₂ molecules, corresponding to a bifunctional activation of the molecule by Lewis basic and Lewis acidic entities. The ambiphilic nature of carbon dioxide makes it an ideal candidate for FLP-type activation.¹² Quickly after the pioneering disclosure of the FLP concept on H₂ activation, the FLP activation was explored for CO₂.^{12a,c,d} This process was then exploited for the trapping and reactivity of CO₂. However, while the FLP concept was recently extended to single electron transfer between the frustrated donor and acceptor counterparts,¹³ the one-electron-reduction of FLP-activated CO₂ has seldom been investigated. To the best of our knowledge, only the (*t*-Bu)₃P–CO₂–B(C₆F₅)₃ adduct was subjected to one-electron reduction by Heiden *et al.*, in a broader investigation on the role of main group elements in CO₂ reduction.¹⁰ They studied the reduction of the (*t*-Bu)₃P–CO₂–B(C₆F₅)₃ adduct by means of DFT, electro- and chemical-reduction (Chart 1b). The DFT study indicated that the mono-reduced species is a minimum on the energy surface with an unpaired spin density of 16% on the carbon of the CO₂ unit.

^aLCC-CNRS, Université de Toulouse, CNRS, 205 route de Narbonne, 31077 Toulouse Cedex 04, France. E-mail: olivier.basle@lcc-toulouse.fr; sebastien.bontemps@lcc-toulouse.fr

^bDepartament de Química, Universitat Autònoma de Barcelona, 08193 Cerdanyola del Valles, Catalonia, Spain. E-mail: agusti.ledos@uab.cat

† Electronic supplementary information (ESI) available. CCDC 2306774–2306777. For ESI and crystallographic data in CIF or other electronic format see DOI: <https://doi.org/10.1039/d3sc06325a>



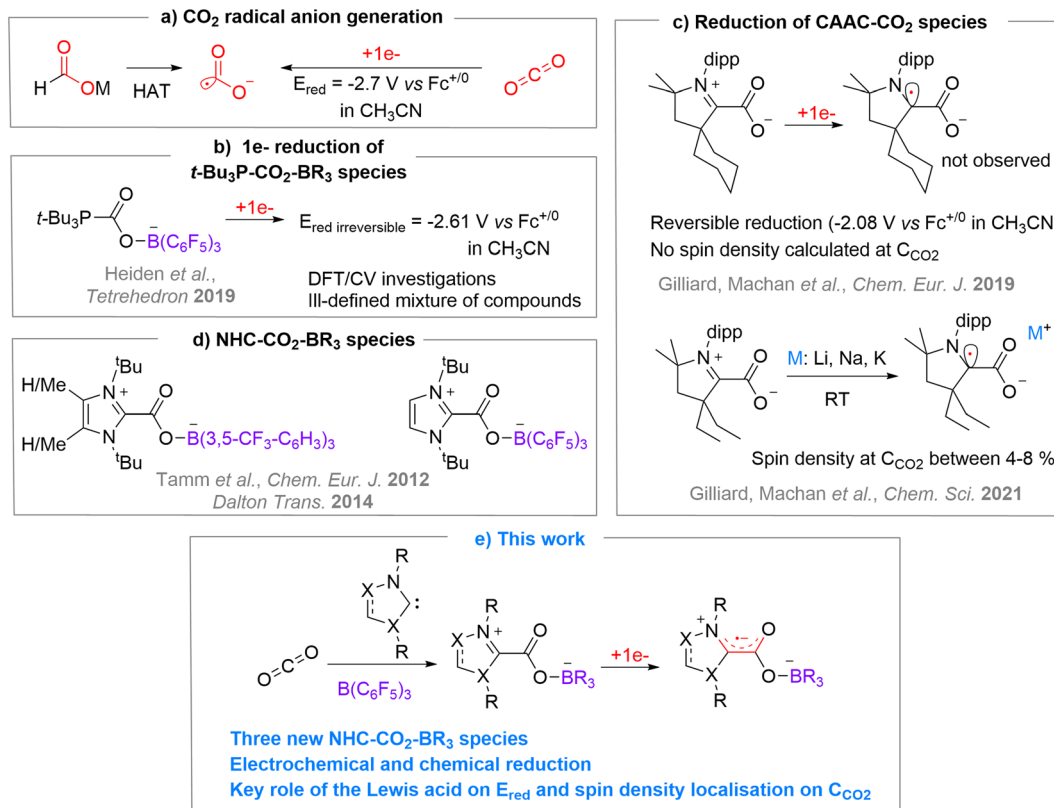


Chart 1 (a) Common strategies to generate [CO₂^{•-}], (b) study of the one-electron reduction of t-Bu₃P-CO₂-B(C₆F₅)₃, (c) one-electron reduction of CAAC-CO₂ species, (d) NHC-CO₂-borane species, (e) synthesis and one-electron reduction of NHC-CO₂-B(C₆F₅)₃ compounds.

However, the electroreduction of (t-Bu)₃P-CO₂-B(C₆F₅)₃ gave rise to irreversible waves at rather low potential of -2.56 V and -2.61 V vs. Fc⁺⁰ in THF and acetonitrile, respectively while the chemical reduction led to an ill-defined mixture of products.

In order to explore the monoelectronic reduction of CO₂ when activated by an FLP system, we turned our attention to N-heterocyclic carbenes (NHCs) as Lewis bases because of their high electronic and steric modularity and also because of their known ability to stabilise radical species.¹⁴ Applied to CO₂, Machan, Gilliard *et al.* have shown that CAAC-CO₂ adducts could be reduced by one electron (Chart 1c), either by cyclic voltammetry in a reversible manner at -2.08 V vs. Fc⁺⁰ in CH₃CN and -2.15 V vs. Fc⁺⁰ in THF for ^{Cy}CAAC,¹⁵ or by alkali metals (Li, Na, K) for ^{Et}CAAC.¹⁶ Interestingly, the calculated unpaired spin density of [CAAC-CO₂^{•-}] highlights the importance of the CAAC moiety in the reduction process, since most of the added density is located on the carbenic carbene and barely any density on the carbon atom of the CO₂ moiety with a maximum of 8%.^{15,16} One can notice, though, that the evaluation of the single electron reduction of other NHC-CO₂ adducts with more classical NHCs is lacking.¹⁷ On the other hand, very few NHCs have been used in FLP-CO₂ activation. To the best of our knowledge, only three examples were reported by Tamm *et al.*¹⁸ in their study concerning the ability of NHC/borane systems to trap CO₂ and N₂O whether the Lewis pair was frustrated or not^{12d,18} (Chart 1d).

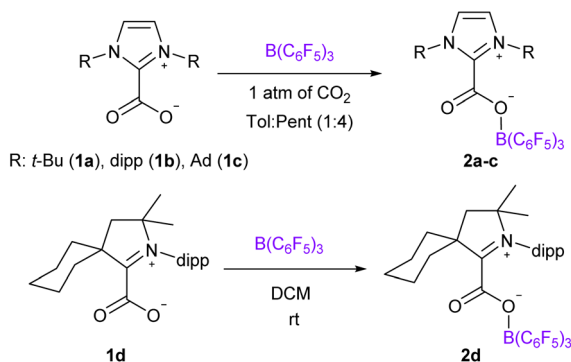
Herein, we report the expansion of the NHC-CO₂-borane library and the exploration of their single electron reduction

leading to reversible or irreversible reduction depending on the nature of the NHC (Chart 1e). Two radical anion FLP-CO₂ systems could be characterized by EPR spectroscopy and one crystallized. The combined theoretical investigations enabled us to scrutinize the reduction potential of these species and the localisation of the unpaired spin density.

Results and discussion

We chose to use tris(pentafluorophenyl)borane (B(C₆F₅)₃) as the Lewis acid and varied the NHC Lewis base to prepare four NHC-CO₂-B(C₆F₅)₃ molecules **2a-d**. We reproduced the synthesis of the adduct **2a**, described by Tamm *et al.*, featuring 1,3-di-*tert*-butylimidazol-2-ylidene (*It*-Bu) and B(C₆F₅)₃ by reacting the *It*Bu-CO₂ adduct **1a** with the borane.^{18a} Following a similar strategy, the NHC-CO₂-B(C₆F₅)₃ systems **2b-d** were synthesized from the reaction between the NHC-CO₂ adducts **1b-d** of 1,3-bis(2,6-diisopropylphenyl)imidazol-2-ylidene (IPr, **1b**), 1,3-bis(1-adamantyl)imidazol-2-ylidene (IAd, **1c**),¹⁹ and cyclohexyl cyclic (alkyl)(amino)carbenes (^{Cy}CAAC, **1d**) and an equimolar amount of B(C₆F₅)₃ under a CO₂ atmosphere (Scheme 1). The adducts **2b-d** were fully characterized by NMR and IR spectroscopy. Overall, these compounds exhibit similar signatures compared to **2a**. In the ¹³C{¹H} NMR spectra, the resonances for the carbon atoms of the CO₂ moiety appear at δ = 156.0, 152.8, 161.1 and 158.0 ppm for **2a-d**, respectively, which represents a de-shielding of approximately 30 ppm compared to free CO₂,





Scheme 1 Synthesis of compounds 2a–d.

In the ^{11}B NMR spectra, the tetrahedral boron atom displays characteristic resonance at $\delta = -3.9$, -3.4 , -3.8 and -2.9 ppm for **2a–d**, respectively. In the solid-state, the IR analysis indicates C=O stretching frequencies at 1714, 1717, 1715 and 1709 cm^{-1} for **2a–d**, respectively (Table 1). These values are included in the large range of FLP- CO_2 molecules ($1645 < \nu(\text{C}=\text{O}) < 1742$ cm^{-1}).^{12b} As a comparison, the antisymmetric O=C=O stretching frequency of CO_2 appears at 2349 cm^{-1} .²⁰ Theoretical investigations revealed that the bands observed at slightly lower frequencies correspond to the $\nu(\text{C}=\text{C})$ and $\nu(\text{C}-\text{F})$ (Table 1 and ESI†). In the case of **2a** for example, these bands were observed at 1644 and 1513 cm^{-1} , respectively.

The solid-state structures were further analysed by single crystal X-ray diffraction analysis (Fig. 1). Selected structural parameters of **2b–d** as well as the comparison with **2a** are reported in Table 2. In all four cases, the incorporation of the CO_2

Table 1 Selected IR stretching frequencies of compounds 2a–d and CO_2

IR stretching frequencies (cm^{-1})	$\nu(\text{C}=\text{O})$	$\nu(\text{C}=\text{C})$	$\nu(\text{C}-\text{F})$
2a	1714	1644	1513
2b	1717	1643	1514
2c	1715	1645	1514
2d	1709	1624	1514
Free CO_2	2736 ^a		

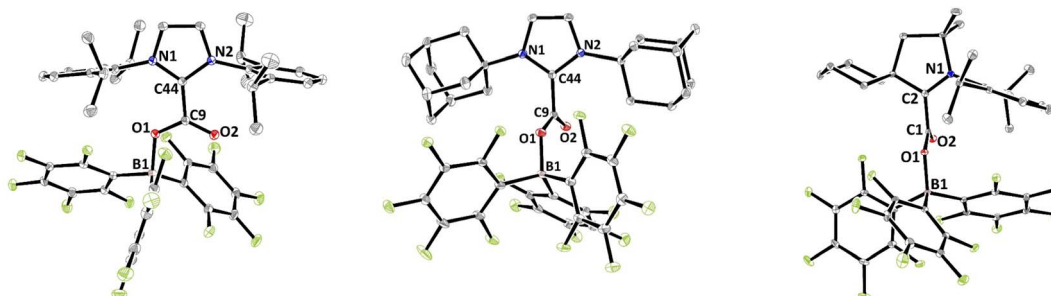
^a ν_{asym} .

Table 2 Structural parameters of $\text{NHC}-\text{CO}_2-\text{B}(\text{C}_6\text{F}_5)_3$ (**2a–d**)

Structural parameters	2a ^{18a}	2b	2c	2d
$d(\text{C}=\text{O})/\text{\AA}$	1.2024(19)	1.2074(18)	1.207(3)	1.2070(17)
$d(\text{C}-\text{O})/\text{\AA}$	1.2972(19)	1.2980(17)	1.298(3)	1.2977(17)
$d(\text{O}-\text{B})/\text{\AA}$	1.535(2)	1.5363(18)	1.540(3)	1.5492(18)
$d(\text{C}_{\text{carbenic}}-\text{CO}_2)/\text{\AA}$	1.516(2)	1.5071(19)	1.523(3)	1.5247(19)
$\alpha(\text{CO}_2)/^\circ$	130.09(15)	128.78(13)	129.96(19)	129.31(13)
$D(\text{NHC}-\text{CO}_2)/^\circ$	80.5(2)	7.3(2)	76.7(3)	79.2(2)

molecule in the FLP systems resulted in its bending with OCO angles comprised between $130.09(15)^\circ$ for **2a** and $128.78(13)^\circ$ for **2b** and with a significant lengthening of the carbon–oxygen bonds leading to an ester like trigonal planar geometry. The structures of **2a–d** feature similar parameters, except for the dihedral angle between the plane of the CO_2 and the plane of the NHC moieties, noted $D(\text{NHC}-\text{CO}_2)$ in Table 2. In fact, while structures **2a**, **2c** and **2d** show torsion angles of $80.5(2)$, $76.7(3)$ and $79.2(2)^\circ$, respectively, the CO_2 moiety and the imidazole ring are almost coplanar in **2b** with a dihedral angle of $7.3(2)^\circ$. These data can be correlated with the $\text{C}_{\text{NHC}}-\text{C}_{\text{CO}_2}$ bond distances, which are longer for **2a**, **2c** and **2d** (1.516(2), 1.52071(19), and 1.5223(3) \AA , respectively) than for the adduct **2b** (1.5071(19) \AA). This feature is in accordance with data gathered on $\text{NHC}-\text{CO}_2$ adducts showing that the C–C bond distance between the carbenic carbon (C_{NHC}) and the CO_2 carbon (C_{CO_2}) is larger with a greater dihedral angle. These C–C distances and torsion angles have then been correlated with the temperature of decarboxylation which is lower with higher dihedral angles and longer C–C distances.²¹

The redox chemistry of species **2a–d** was probed by cyclic voltammetry experiments at room temperature in dry dichloromethane ($n\text{Bu}_4\text{PF}_6$, 0.1 M) to ensure good solubility. Satisfyingly, the reduction of adducts **2a–d** led to clear waves depicted in Fig. 2 with reduction potentials expressed vs. $\text{Fc}^{+/0}$. The cyclic voltammograms of **2a** (orange wave) and **2c** (blue wave) show irreversible reduction at $E_{\text{p}}^{\text{red}} = -2.30$ V and -2.44 V, respectively. Although, upon reduction, the related (*t*-Bu)₃P- $\text{CO}_2-\text{B}(\text{C}_6\text{F}_5)_3$ and $^{\text{Cy}}\text{CAAC}-\text{CO}_2$ led to interesting CO_2 disproportionation transformations under certain conditions,^{10,15} we did not explore further the fate of the reduced **2a** and **2c**. The cyclic voltammogram of **2b** (brown wave) reveals a quasi-reversible reduction at $E_{1/2} = -2.08$ V ($\Delta E_{\text{p}} = 150$ mV). Finally,

Fig. 1 Structures of compounds **2b** (left), **2c** (middle) and **2d** (right). Thermal ellipsoids drawn at 30% probability.

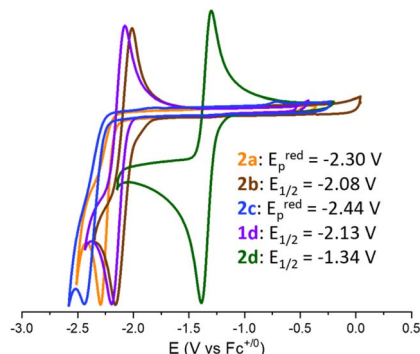


Fig. 2 Normalized cyclic voltammograms of NHC-CO₂-B(C₆F₅)₃ adducts **1d** and **2a-d** on a GC microdisk in 0.1 M [*n*Bu₄N][PF₆]/CH₂Cl₂ media under an Ar atmosphere (5 × 10⁻³ M of adduct, rt, scan rate: 0.2 V s⁻¹).

the quasi-reversible one-electron reduction of compound **2d** (green wave) occurs at a potential of $E_{1/2} = -1.34$ V ($\Delta E_p = 90$ mV). The reduction potential of compound **1d** was also recorded at $E_{1/2} = -2.13$ V ($\Delta E_p = 132$ mV), in accordance with the data reported in the literature.¹⁵ Overall, the recorded E^{red} data indicate that compounds **2a-d** featuring an FLP-type activated molecule of CO₂ are more easily reduced by one electron than free CO₂. The most important gain is obtained with the combination of CAAC and B(C₆F₅)₃ enabling the achievement of a remarkable reduction potential $E_{1/2}$ of -1.34 V in CH₂Cl₂ compared to free CO₂ (*i.e.*, $E_p^{\text{red}} = -2.65$ V in DMF, -2.70 V in CH₃CN and -2.53 V in aqueous solution *vs.* Fc^{+/₀}).^{8b,10} The less negative reduction potential observed in the case of CAAC *vs.* the more classical NHC probably results from the higher π -accepting ability of CAAC, which is the consequence of a more accessible LUMO orbital.²² This feature would thus indicate that

the reduction event is at least partially localised on the carbenic carbon, which is confirmed by the following experimental and theoretical investigations. The beneficial role of the borane – which was expected because it decreases the electronic density from the carbene-CO₂ adduct – is quantified by a net gain of 0.79 V observed between the $E_{1/2}$ of **2d** compared to that of **1d**.

In order to gain further insights into the role of the NHC/borane pair in the activation of CO₂, DFT calculations were undertaken using the M06-2X functional combined with Grimme's D3 correction to consider dispersion effects (see Computational details in the ESI†). The structures of **2a-d** and of NHC-CO₂ adducts **1a-d** were computed. In addition, the structures of **2(a-d)-BH₃**, featuring BH₃ in place of B(C₆F₅)₃ were also computed as models for a less Lewis acidic borane. The calculated charges by Natural Population Analysis (NPA) on the C_{CO₂} reflect the electron withdrawing effect of the borane to a moderate extent (Table S9†). For example, the NPA charge of **1a** is 0.75*e* and is 0.81*e* for **2a**, while the NPA charge of the C_{CO₂} of free CO₂ is significantly more positive (1.05). Similar variations of 0.05 to 0.09*e* are observed in the case of the other NHC. The LUMO orbitals of the series were also analysed (Fig. 3). In the adducts **1a-d** the π -type LUMOs are mostly located on the carbenic centres, which is in line with the less negative reduction potentials observed for the CAAC adducts. The addition of borane (BH₃ and B(C₆F₅)₃) leads to the delocalisation of the LUMO over the C_{CO₂} as well. This phenomenon is enhanced with the increased Lewis acidity of B(C₆F₅)₃ *vs.* BH₃. The role of the dihedral angle $D(\text{NHC-CO}_2)$ was also explored. Relaxed potential energy scans were computed for the rotation, carrying out constrained optimisations for each value of the dihedral angle (see Fig. S76†). From them, a minimum and rotational transition states were located for each structure. In each case, the minimum corresponds to the relative orientation of the NHC and CO₂ moieties observed in the crystal

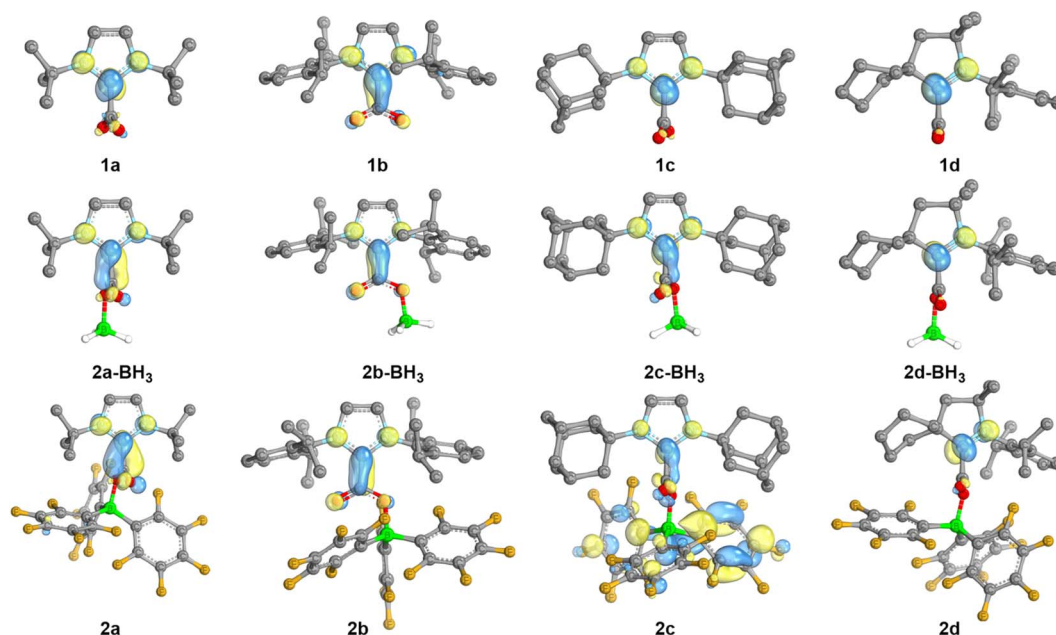


Fig. 3 LUMO orbitals of the neutral NHC-based adducts. Visualization (IBOview,²³ threshold = 45) with colour code: carbon (grey), nitrogen (light blue), boron (green), fluorine (dark yellow), oxygen (red).



structures: orthogonal in the case of **2a**, **2c-d**, and coplanar for **2b**. Computations also evidenced these preferences in the absence of borane and with BH_3 , since the NHC and CO_2 moieties are also found orthogonal for **1a**, **1c-d**, as well as for the corresponding BH_3 adducts and coplanar for **1b** and **2b-BH₃**. These features suggest that the observed variations between **2** and **2-BH₃** stem mostly from the difference in the electronic properties between $\text{B}(\text{C}_6\text{F}_5)_3$ and BH_3 of lower Lewis acidity and not from steric differences. The barriers of rotation of **2a-d** were evaluated to be accessible at room temperature since the highest is calculated at $16.5 \text{ kcal mol}^{-1}$. The barrier for **2b** ($4.6 \text{ kcal mol}^{-1}$) is significantly smaller compared to the one for **2a**, **2c** and **2d** (13.5 , 16.5 and $11.8 \text{ kcal mol}^{-1}$, respectively).

Reduction potentials of compounds **2a-d** were computed accurately with maximum deviation from the experimental values of 0.14 V . However, the calculated potential for **1d** is off by 0.25 V (*vide infra* for the proposed explanation). We then explored the effect of the borane on the reduction potential. As for **1d** vs. **2d**, the absence of borane in **1a-c** has a significant impact with calculated potentials of -3.42 , -3.00 and -3.44 V vs. $\text{Fc}^{+/0}$, respectively. These values are more negative than that of free CO_2 , explaining the absence of any reduction potential values for the classical NHC- CO_2 adduct in the literature.^{17a}

Having calculated that the relative rotations of NHC and $\text{CO}_2\text{-B}(\text{C}_6\text{F}_5)_3$ moieties are accessible at room temperature, we wondered if the reduction potentials vary with the dihedral angle. Transition states $[\mathbf{1d}]^\ddagger$ and $[\mathbf{2a-d}]^\ddagger$ were found resulting from the rotation of the NHC and CO_2 moieties in **1d** and **2a-d**, respectively. The calculated values indicate that indeed the reduction potential is sensitive to the dihedral angle since much less negative potentials were calculated for these TS (Table 3), in line with the fact that the LUMOs are lower in energy after rotation (Fig. S76†). Nonetheless, the values calculated for $[\mathbf{2a-d}]^\ddagger$ do not correspond to the experimental values suggesting that it is indeed **2a-d** that are reduced in the CV and not $[\mathbf{2a-d}]^\ddagger$. However, in the case of $[\mathbf{1d}]^\ddagger$, the calculated potential is significantly closer to the experimental value ($\Delta = 0.04$ vs. 0.25 V), which could indicate that it is in fact the reduction of $[\mathbf{1d}]^\ddagger$ that is measured experimentally. Further exploration aiming at controlling the degree of rotation would nonetheless be necessary to confirm this hypothesis.

In addition to electrochemical studies, we investigated the chemical reduction of adducts **2a-d** with one equivalent of potassium graphite (KC_8) as the chemical reductant in THF under argon. In accordance with the irreversible waves observed for **2a** and **2c**, no radical species could be detected upon chemical reduction. However, the reduction of **2b** and **2d** at 298

K led to a deep red and yellow solution, respectively, exhibiting EPR signals. As shown in Fig. 4b, five ($g = 2.0026$) and three ($g = 2.0026$) hyperfine lines were observed for $[\mathbf{2b}^{\cdot-}]$ and $[\mathbf{2d}^{\cdot-}]$, respectively, indicative of a radical electron coupling with the two equivalent nitrogen nuclei ($a_{\text{N}} = 4.6 \text{ G}$) for $[\mathbf{2b}^{\cdot-}]$ and one nitrogen nucleus ($a_{\text{N}} = 6.1 \text{ G}$) for $[\mathbf{2d}^{\cdot-}]$. DFT calculation reproduced the EPR signals accurately (Fig. S66 and S67†). In accordance with the reduction potential measured at -1.34 V for **2d**, $[\mathbf{2d}^{\cdot-}]$ could also be generated using $\text{Co}(\text{Cp}^*)_2$ as a milder reductant ($E_{\text{red}} = -1.94 \text{ V}$ vs. $\text{Fc}^{+/0}$ in CH_2Cl_2), as proved by the observation of a very similar EPR signal (Fig. S69†). These radical species are stable in solution under an inert argon atmosphere at room temperature, at least for two days as shown by EPR analyses (Fig. S66 and S67†). IR frequency involving the C=O bond was measured at 1596 cm^{-1} in the solid state for the isolated $[\mathbf{2d}^{\cdot-}]$, while only the solution IR frequency was recorded for the *in situ* generated $[\mathbf{2b}^{\cdot-}]$. DFT calculations indicate that these frequencies correspond to the combination of the stretching of the C=O and C-C_{NHC} bonds (ESI†). While attempts to obtain crystals were unsuccessful with the radical $[\mathbf{2b}^{\cdot-}]$, single crystals of $[\mathbf{2d}^{\cdot-}][\text{K}^+](\text{THF})_2$, suitable for X-ray diffraction, were grown from a concentrated THF/pentane solution at $-35 \text{ }^\circ\text{C}$. In comparison with the structural parameters of the parent neutral form **2d**, the additional electron in $[\mathbf{2d}^{\cdot-}]$ is responsible for important changes. The most striking difference concerns the torsion between the plane of the CO_2 moiety and the plane of the CAAC ring, which, from a dihedral angle of $79.2(2)^\circ$ in **2d**, reaches a minimum in $[\mathbf{2d}^{\cdot-}]$ with a dihedral angle of $0.1(3)^\circ$. This phenomenon was also observed in the absence of borane by Machan, Gilliard *et al.* and highlights the increased resonance between the NHC and the CO_2 fragments in the reduced form. In line, important shortening of the C_{NHC}-C_{CO₂} bond [$1.433(3) \text{ \AA}$] and the O-B bond [$1.486(3) \text{ \AA}$] is witnessed in $[\mathbf{2d}^{\cdot-}]$, along with lengthening of the N-C_{NHC} [$1.374(3) \text{ \AA}$], C=O [$1.241(3) \text{ \AA}$] and C-O [$1.331(2) \text{ \AA}$] bonds. In addition, the bending of the CO_2 moiety is enhanced reaching an angle of $122.26(18)^\circ$ (vs. $129.31(13)$ for **2d**, Fig. 4d). This bending is very similar to the bending observed in the reduction of the CAAC- CO_2 adduct with Li, Na and K leading to a bending of $122.9(2)^\circ$ with Na to $123.71(9)^\circ$ for Li.¹⁶ DFT calculations were conducted on $[\text{NHC-CO}_2\text{-BR}_3^{\cdot-}]$ and $[\text{NHC-CO}_2^{\cdot-}]$ adducts and indicate that the coplanar rearrangement of the NHC and CO_2 planes is a general phenomenon since it is predicted for the all series of $[\text{NHC-CO}_2\text{-BR}_3^{\cdot-}]$ and $[\text{NHC-CO}_2^{\cdot-}]$ adducts (Fig. 4c and ESI†). All cases feature separated anionic and radical sites and can thus be described as distonic anions. While as in $[\text{CO}_2^{\cdot-}]$ the anionic charge is mostly located on the oxygen

Table 3 Calculated and experimental (in brackets) reduction potentials vs. $\text{Fc}^{+/0}$ for compounds **1a-d**, **2a-d**, **1d_{rot}** and **2a-d_{rot}**

Compounds	a	b	c	d
1	-3.42	-3.00	-3.44	-2.38 (-2.13)
2	-2.26 (-2.30)	-2.04 (-2.08)	-2.30 (-2.44)	-1.29 (-1.34)
$[\mathbf{1}]^\ddagger$	—	—	—	-2.09 ^a
$[\mathbf{2}]^\ddagger$	-1.68 ^a	-1.84 ^b	-1.58 ^a	-0.78 ^a

^a Coplanar TS. ^b Orthogonal TS.



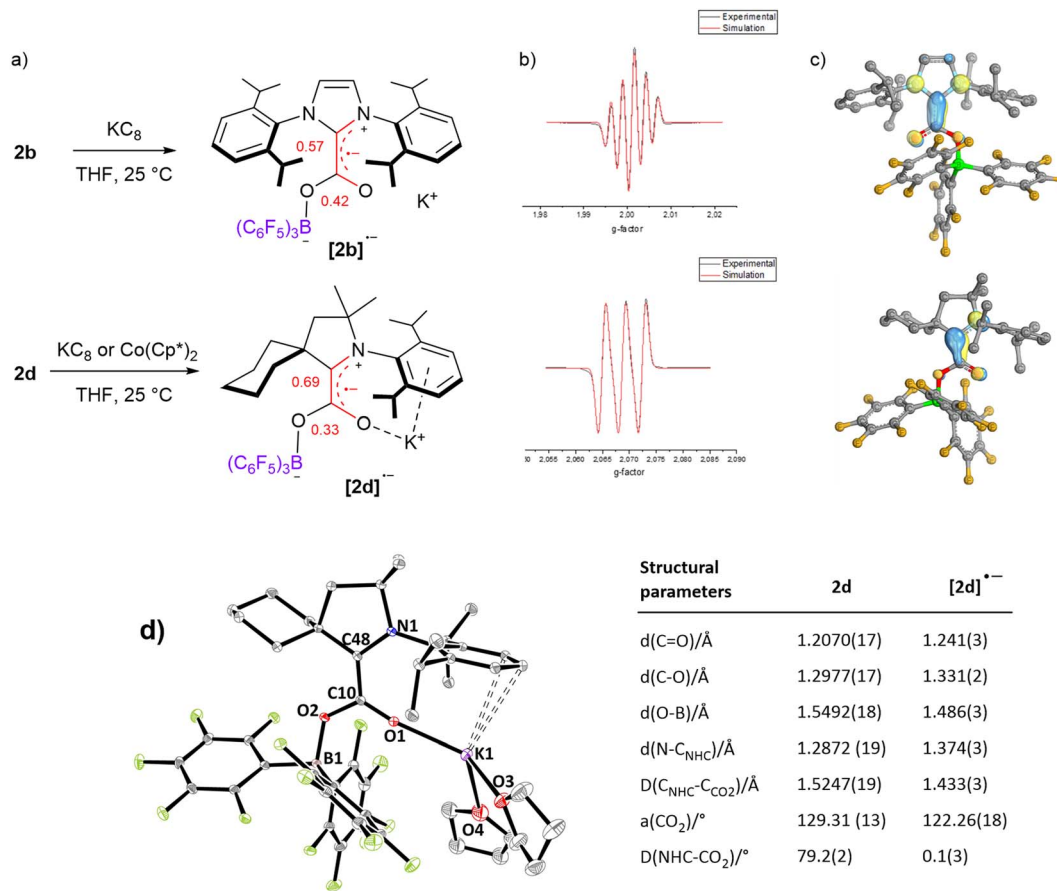


Fig. 4 Characterization of the radical anions [2b]^{•-} and [2d]^{•-}: (a) mono-reduction of 2b and 2d into [2b]^{•-} and [2d]^{•-}, (b) experimental (black) and simulated (red) EPR spectra, (c) calculated SOMO orbitals, (d) solid-state structure of [2d]^{•-}[K⁺](THF)₂ and selected structural parameters of [2d]^{•-}.

atoms, the radical charge is however mostly located on the C_{NHC} in the case of [1a-d]^{•-} compounds and not on the C_{CO₂}. Moreover, the radical resides in a π-type orbital instead of a σ-type orbital in [CO₂^{•-}]. Interestingly, the addition of a borane enables transferring of a part of the unpaired spin density to the C_{CO₂} in [2(a-d)-BH₃^{•-}] and [2a-d]^{•-}, which is slightly closer to the [CO₂^{•-}] situation. In more detail, the localized Mulliken atomic spin density of [2b]^{•-} and [2d]^{•-} indicates a large distribution on the C_{NHC} (0.57 and 0.69, respectively) and on the C_{CO₂} (0.42 and 0.33, respectively), while lower spin density is found on the nitrogen (0.17, 0.23, respectively) and on the oxygen (0.14, 0.12, respectively) atoms. The portion of spin density found on the C_{CO₂} of [2b]^{•-} and [2d]^{•-} is remarkable when taking into account the absence of any calculated spin density on the C_{CO₂} of the mono-reduced form of the ^{cy}CAAC-CO₂ adduct [1d]^{•-} (Table S8†).¹⁵ It is in line with the spin density calculation of Heiden *et al.* on the parent [t-Bu₃P-CO₂-B(C₆F₅)₃]^{•-} adduct with 16% on C_{CO₂}, but to a larger extent.¹⁰

As a preliminary evaluation of the reactivity of the radical anionic species [2b]^{•-} and [2d]^{•-}, we wished to probe their reactivity with DMPO since this is a classical trapping agent for

[CO₂^{•-}], giving rise to a very characteristic EPR signal featuring six bands at $g = 2.0058$ ($a_N = 15.8$ G, $a_{\beta-H} = 19.1$ G) in aqueous media (Table 4, entry 1).⁴ Satisfyingly, when [2b]^{•-} and [2d]^{•-} were reacted with five equivalents of DMPO, the EPR signals of [2b]^{•-} and [2d]^{•-} were replaced by a similar sextet at $g = 2.0052$ ($a_N = 14.0$ G and $a_{\beta-H} = 18.6$ G) and $g = 2.0050$ ($a_N = 14.4$ G and $a_{\beta-H} = 20.0$ G), respectively (Table 4, entries 2 and 3, Fig. S71†). A loss of signal intensity is however observed, presumably due to stability issues under these conditions. In the absence of borane, the chemically reduced compound [1d]^{•-} also reacts

Table 4 Experimental and computed EPR data

Entries	[DMPO-CO ₂ ^{•-}]	g	a_N /G	$a_{\beta-H}$ /G
1	Ref 1a ^a	2.0058	15.8	19.1
2	From [2b] ^{•-}	2.0052	14.0	18.6
3	From [2d] ^{•-}	2.0050	14.4	20.0
4	From [1d] ^{•-}	2.0050	15.0	20.1
5	Calculated by DFT	2.0080	13.7	22.3
6	Calculated by DFT with B(C ₆ F ₅) ₃	2.0081	13.7	21.8

^a In H₂O.



like $[\text{CO}_2^{\cdot-}]$ toward DMPO as indicated by a similar EPR signal at $g = 2.0050$ ($a_{\text{N}} = 15.0$ G and $a_{\beta\text{-H}} = 20.1$ G), (Fig. S71†). This is in line with the observation that when $[\mathbf{1d}^{\cdot-}]$ was generated electrochemically under a CO_2 atmosphere by Gilliard, Machan *et al.*, a disproportionation reaction was observed, which is a known reactivity of $[\text{CO}_2^{\cdot-}]$.¹⁵ At this stage, it is difficult to assess whether or not the borane moiety is maintained in the products of these spin trapping experiments. As indicated by DFT calculations, $[\text{DMPO-CO}_2^{\cdot-}]$ and $[\text{DMPO-CO}_2\text{-B}(\text{C}_6\text{F}_5)_3^{\cdot-}]$ would afford similar EPR signals (Table 4, entries 5 and 6). Further studies will be necessary to understand and exploit the reactivity of the monoreduced FLP-type activated CO_2 molecules in valuable synthetic strategies.

Conclusions

Three new NHC- $\text{CO}_2\text{-B}(\text{C}_6\text{F}_5)_3$ adducts **2b–d** are reported. The one-electron reduction of these adducts and of the known adduct *It*-Bu- $\text{CO}_2\text{-B}(\text{C}_6\text{F}_5)_3$ **2a**, shows reversible and irreversible waves depending on the nature of the NHC. This combined experimental and theoretical study highlights the beneficial role of the FLP-type activation of CO_2 with NHC/ BR_3 pair for the one electron redox event. The LUMOs of the NHC- $\text{CO}_2\text{-B}(\text{C}_6\text{F}_5)_3$ adducts are mostly located on the C_{NHC} which was shown to be the main site of reduction. The adduct **2d** featuring a π -accepting CAAC exhibits less negative reduction potential than adducts with more classical NHCs. DFT calculations highlighted the role of the dihedral angle between the carbene and CO_2 moieties and of the borane in the reduction potential. The withdrawing effect of the Lewis acidic borane was indeed shown to lead to a less negative reductive potential ($E_{1/2} = -1.34$ V vs. $\text{Fc}^{+/0}$ for **2d**). Furthermore, the two species exhibiting reversible waves in the CV experiment were shown to afford stable anionic radical species by chemical reduction, which could be characterised by EPR for $[\mathbf{2b}^{\cdot-}]$ and $[\mathbf{2d}^{\cdot-}]$ and X-ray diffraction analysis for $[\mathbf{2d}^{\cdot-}]$. In these distonic species, the radical site was shown to be located not only on the C_{NHC} but also on the C_{CO_2} with a maximum spin density on the C_{CO_2} of 0.42 for $[\mathbf{2b}^{\cdot-}]$. Finally, $[\mathbf{2b}^{\cdot-}]$ and $[\mathbf{2d}^{\cdot-}]$ were shown to exhibit a reactivity similar to $[\text{CO}_2^{\cdot-}]$ toward DMPO. Future studies will further explore the reactivity of the stable and unstable radical anions of type $[\mathbf{2}^{\cdot-}]$, as well as the broader use of FLP-type activation of carbon dioxide in single electron reduction transformations.

Data availability

Raw data of NMR, CV, EPR and X-ray crystallography are available upon reasonable request.

Author contributions

AM conducted the theoretical and experimental work. CG conducted the experimental work. AS-S and LV conducted CV and X-ray diffraction analyses, respectively. AL, OB and SB conceptualised the project and supervised the experimental and theoretical work. All authors participated in writing, reviewing and editing the original draft.

Conflicts of interest

There are no conflicts to declare.

Acknowledgements

This research has received funding from the European Union's Horizon 2020 research and innovation programme under the Marie Skłodowska-Curie grant agreement no. 860322. We acknowledge the valuable support of the NMR service and EPR platform at LCC-CNRS. Calculations on this project were carried out with the use of CSUC supercomputing resources. We thank Vincent César and Nicolas Queyriaux for fruitful discussions.

References

- (a) F. A. Villamena, E. J. Locigno, A. Rockenbauer, C. M. Hadad and J. L. Zweier, Theoretical and Experimental Studies of the Spin Trapping of Inorganic Radicals by 5,5-Dimethyl-1-Pyrroline N-Oxide (DMPO). 1. Carbon Dioxide Radical Anion, *J. Phys. Chem. A*, 2006, **110**, 13253–13258; (b) J. R. Harbour and M. L. Hair, Spin trapping of the $\cdot\text{CO}_2^-$ radical in aqueous medium, *Can. J. Chem.*, 1979, **57**, 1150–1152.
- D. C. Grills and S. V. Lyman, Radiolytic formation of the carbon dioxide radical anion in acetonitrile revealed by transient IR spectroscopy, *Phys. Chem. Chem. Phys.*, 2018, **20**, 10011–10017.
- A. Herburger, M. Ončák, C.-K. Siu, E. G. Demissie, J. Heller, W. K. Tang and M. K. Beyer, Infrared Spectroscopy of Size-Selected Hydrated Carbon Dioxide Radical Anions $\text{CO}_2^{\cdot-}(\text{H}_2\text{O})_n$ ($n=2\text{--}61$) in the C–O Stretch Region, *Chem. – Eur. J.*, 2019, **25**, 10165–10171.
- N. J. Firet and W. A. Smith, Probing the Reaction Mechanism of CO_2 Electroreduction over Ag Films via Operando Infrared Spectroscopy, *ACS Catal.*, 2017, **7**, 606–612.
- M. E. Jacox and W. E. Thompson, The vibrational spectra of molecular ions isolated in solid neon. I. CO_2^+ and CO_2^- , *J. Chem. Phys.*, 1989, **91**, 1410–1416.
- D. Schröder, C. A. Schalley, J. N. Harvey and H. Schwarz, On the formation of the carbon dioxide anion radical $\text{CO}_2^{\cdot-}$ in the gas phase, *Int. J. Mass Spectrom.*, 1999, **185–187**, 25–35.
- S. J. Yu, C. L. Holliman, D. L. Rempel and M. L. Gross, The β -distonic ion from the reaction of pyridine radical cation and ethene: a demonstration of high-pressure trapping in Fourier transform mass spectrometry, *J. Am. Chem. Soc.*, 1993, **115**, 9676–9682.
- (a) A. Malandain, M. Molins, A. Hauwelle, A. Talbot, O. Loreau, T. D'Anfray, S. Goutal, N. Tournier, F. Taran, F. Caillé and D. Audisio, Carbon Dioxide Radical Anion by Photoinduced Equilibration between Formate Salts and $[\text{C}^{11}\text{C}, \text{C}^{13}\text{C}, \text{C}^{14}\text{C}]\text{CO}_2$: Application to Carbon Isotope Radiolabeling, *J. Am. Chem. Soc.*, 2023, **145**, 16760–16770; (b) Y. You, W. Kanna, H. Takano, H. Hayashi, S. Maeda and T. Mita, Electrochemical Dearomative Dicarboxylation of Heterocycles with Highly Negative Reduction Potentials, *J. Am. Chem. Soc.*, 2022, **144**, 3685–3695; (c) L. Song,



- W. Wang, J.-P. Yue, Y.-X. Jiang, M.-K. Wei, H.-P. Zhang, S.-S. Yan, L.-L. Liao and D.-G. Yu, Visible-light photocatalytic di- and hydro-carboxylation of unactivated alkenes with CO₂, *Nat. Catal.*, 2022, **5**, 832–838; (d) L.-L. Liao, Z.-H. Wang, K.-G. Cao, G.-Q. Sun, W. Zhang, C.-K. Ran, Y. Li, L. Chen, G.-M. Cao and D.-G. Yu, Electrochemical Ring-Opening Dicarboxylation of Strained Carbon–Carbon Single Bonds with CO₂: Facile Synthesis of Diacids and Derivatization into Polyesters, *J. Am. Chem. Soc.*, 2022, **144**, 2062–2068; (e) J.-H. Ye, T. Ju, H. Huang, L.-L. Liao and D.-G. Yu, Radical Carboxylative Cyclizations and Carboxylations with CO₂, *Acc. Chem. Res.*, 2021, **54**, 2518–2531; (f) T. Ju, Y.-Q. Zhou, K.-G. Cao, Q. Fu, J.-H. Ye, G.-Q. Sun, X.-F. Liu, L. Chen, L.-L. Liao and D.-G. Yu, Dicarboxylation of alkenes, allenes and (hetero)arenes with CO₂ via visible-light photoredox catalysis, *Nat. Catal.*, 2021, **4**, 304–311; (g) H. Huang, J.-H. Ye, L. Zhu, C.-K. Ran, M. Miao, W. Wang, H. Chen, W.-J. Zhou, Y. Lan, B. Yu and D.-G. Yu, Visible-Light-Driven Anti-Markovnikov Hydrocarboxylation of Acrylates and Styrenes with CO₂, *CCS Chem.*, 2021, **3**, 1746–1756; (h) R. Mello, J. C. Arango-Daza, T. Varea and M. E. González-Núñez, Photoiodocarboxylation of Activated C=C Double Bonds with CO₂ and Lithium Iodide, *J. Org. Chem.*, 2018, **83**, 13381–13394; (i) J.-H. Ye, M. Miao, H. Huang, S.-S. Yan, Z.-B. Yin, W.-J. Zhou and D.-G. Yu, Visible-Light-Driven Iron-Promoted Thiocarboxylation of Styrenes and Acrylates with CO₂, *Angew. Chem., Int. Ed.*, 2017, **56**, 15416–15420; (j) H. Seo, A. Liu and T. F. Jamison, Direct β-Selective Hydrocarboxylation of Styrenes with CO₂ Enabled by Continuous Flow Photoredox Catalysis, *J. Am. Chem. Soc.*, 2017, **139**, 13969–13972; (k) H. Seo, M. H. Katcher and T. F. Jamison, Photoredox activation of carbon dioxide for amino acid synthesis in continuous flow, *Nat. Chem.*, 2017, **9**, 453–456; (l) A. Akhgarnusch, R. F. Höckendorf, Q. Hao, K. P. Jäger, C.-K. Siu and M. K. Beyer, Carboxylation of Methyl Acrylate by Carbon Dioxide Radical Anions in Gas-Phase Water Clusters, *Angew. Chem., Int. Ed.*, 2013, **52**, 9327–9330; (m) M. D. Otero, B. Batanero and F. Barba, CO₂ anion–radical in organic carboxylations, *Tetrahedron Lett.*, 2006, **47**, 2171–2173; (n) D. A. Morgenstern, R. E. Wittrig, P. E. Fanwick and C. P. Kubiak, Photoreduction of carbon dioxide to its radical anion by nickel cluster [Ni₃(μ₃-I)₂(dppm)₃]: formation of two carbon-carbon bonds via addition of carbon dioxide radical anion to cyclohexene, *J. Am. Chem. Soc.*, 1993, **115**, 6470–6471; (o) M. Mikhael, S. N. Alektiar, C. S. Yeung and Z. K. Wickens, Translating Planar Heterocycles into Three-Dimensional Analogs by Photoinduced Hydrocarboxylation, *Angew. Chem., Int. Ed.*, 2023, **62**, e202303264; (p) S. N. Alektiar, J. Han, Y. Dang, C. Z. Rubel and Z. K. Wickens, Radical Hydrocarboxylation of Unactivated Alkenes via Photocatalytic Formate Activation, *J. Am. Chem. Soc.*, 2023, **145**, 10991–10997; (q) S. N. Alektiar and Z. K. Wickens, Photoinduced Hydrocarboxylation via Thiol-Catalyzed Delivery of Formate Across Activated Alkenes, *J. Am. Chem. Soc.*, 2021, **143**, 13022–13028; (r) C. M. Hendy, G. C. Smith, Z. Xu, T. Lian and N. T. Jui, Radical Chain Reduction via Carbon Dioxide Radical Anion (CO₂^{•-}), *J. Am. Chem. Soc.*, 2021, **143**, 8987–8992; (s) J. Majhi and G. A. Molander, Recent Discovery, Development, and Synthetic Applications of Formic Acid Salts in Photochemistry, *Angew. Chem., Int. Ed.*, 2023, e202311853; (t) H. Wang, Y. Gao, C. Zhou and G. Li, Visible-Light-Driven Reductive Carboxylation of Styrenes with CO₂ and Aryl Halides, *J. Am. Chem. Soc.*, 2020, **142**, 8122–8129; (u) S. Wang, P. Xu and X. Zhu, CO₂ Radical Anion in Photochemical Dicarboxylation of Alkenes, *ChemCatChem*, 2023, **15**, e202300695.
- 9 (a) P. Xu, X.-Y. Wang, Z. Wang, J. Zhao, X.-D. Cao, X.-C. Xiong, Y.-C. Yuan, S. Zhu, D. Guo and X. Zhu, Defluorinative Alkylation of Trifluoromethylbenzimidazoles Enabled by Spin-Center Shift: A Synergistic Photocatalysis/Thiol Catalysis Process with CO₂^{•-}, *Org. Lett.*, 2022, **24**, 4075–4080; (b) A. F. Chmiel, O. P. Williams, C. P. Chernowsky, C. S. Yeung and Z. K. Wickens, Non-innocent Radical Ion Intermediates in Photoredox Catalysis: Parallel Reduction Modes Enable Coupling of Diverse Aryl Chlorides, *J. Am. Chem. Soc.*, 2021, **143**, 10882–10889; (c) S.-S. Yan, S.-H. Liu, L. Chen, Z.-Y. Bo, K. Jing, T.-Y. Gao, B. Yu, Y. Lan, S.-P. Luo and D.-G. Yu, Visible-light photoredox-catalyzed selective carboxylation of C(sp³)-F bonds with CO₂, *Chem*, 2021, **7**, 3099–3113; (d) O. P. Williams, A. F. Chmiel, M. Mikhael, D. M. Bates, C. S. Yeung and Z. K. Wickens, Practical and General Alcohol Deoxygenation Protocol, *Angew. Chem., Int. Ed.*, 2023, **62**, e202300178.
- 10 B. L. Thompson and Z. M. Heiden, Investigation of main group promoted carbon dioxide reduction, *Tetrahedron*, 2019, **75**, 2099–2105.
- 11 (a) G. Prieto, Carbon Dioxide Hydrogenation into Higher Hydrocarbons and Oxygenates: Thermodynamic and Kinetic Bounds and Progress with Heterogeneous and Homogeneous Catalysis, *ChemSusChem*, 2017, **10**, 1056–1070; (b) J. Luo and I. Larrosa, C–H Carboxylation of Aromatic Compounds through CO₂ Fixation, *ChemSusChem*, 2017, **10**, 3317–3332; (c) J. Klankermayer, S. Wesselbaum, K. Beydoun and W. Leitner, Selective Catalytic Synthesis Using the Combination of Carbon Dioxide and Hydrogen: Catalytic Chess at the Interface of Energy and Chemistry, *Angew. Chem., Int. Ed.*, 2016, **55**, 7296–7343; (d) Q. Liu, L. Wu, R. Jackstell and M. Beller, Using carbon dioxide as a building block in organic synthesis, *Nat. Commun.*, 2015, **6**, 1–15; (e) A. M. Appel, J. E. Bercaw, A. B. Bocarsly, H. Dobbek, D. L. DuBois, M. Dupuis, J. G. Ferry, E. Fujita, R. Hille, P. J. A. Kenis, C. A. Kerfeld, R. H. Morris, C. H. F. Peden, A. R. Portis, S. W. Ragsdale, T. B. Rauchfuss, J. N. H. Reek, L. C. Seefeldt, R. K. Thauer and G. L. Waldrop, Frontiers, Opportunities, and Challenges in Biochemical and Chemical Catalysis of CO₂ Fixation, *Chem. Rev.*, 2013, **113**, 6621–6658; (f) M. Cokoja, C. Bruckmeier, B. Rieger, W. A. Herrmann and F. E. Kühn, Transformation of Carbon Dioxide with Homogeneous Transition-Metal Catalysts: A Molecular Solution to a Global Challenge?, *Angew. Chem., Int. Ed.*, 2011, **50**, 8510–8537.



- 12 (a) M. Pérez-Jiménez, H. Corona, F. de la Cruz-Martínez and J. Campos, Donor-Acceptor Activation of Carbon Dioxide, *Chem. – Eur. J.*, 2023, e202301428; (b) S. Bontemps, Boron-Mediated Activation of Carbon Dioxide, *Coord. Chem. Rev.*, 2016, 308(2), 117–130; (c) D. W. Stephan and G. Erker, Frustrated Lewis Pair Chemistry: Development and Perspectives, *Angew. Chem., Int. Ed.*, 2015, 54, 6400–6441; (d) E. L. Kolychev, E. Theuergarten and M. Tamm, in *Frustrated Lewis Pairs II: Expanding the Scope*, ed. G. Erker and D. W. Stephan, Springer Berlin Heidelberg, Berlin, Heidelberg, 2013, pp. 121–155.
- 13 (a) L. J. C. van der Zee, S. Pahar, E. Richards, R. L. Melen and J. C. Slootweg, Insights into Single-Electron-Transfer Processes in Frustrated Lewis Pair Chemistry and Related Donor-Acceptor Systems in Main Group Chemistry, *Chem. Rev.*, 2023, 123, 9653–9675; (b) Z. Lu, M. Ju, Y. Wang, J. M. Meinhardt, J. I. Martinez Alvarado, E. Villemure, J. A. Terrett and S. Lin, Regioselective aliphatic C–H functionalization using frustrated radical pairs, *Nature*, 2023, 619, 514–520; (c) A. Dasgupta, E. Richards and R. L. Melen, Frustrated Radical Pairs: Insights from EPR Spectroscopy, *Angew. Chem., Int. Ed.*, 2021, 60, 53–65; (d) F. Holtrop, A. R. Jupp, N. P. van Leest, M. Paradiz Dominguez, R. M. Williams, A. M. Brouwer, B. de Bruin, A. W. Ehlers and J. C. Slootweg, Photoinduced and Thermal Single-Electron Transfer to Generate Radicals from Frustrated Lewis Pairs, *Chem. – Eur. J.*, 2020, 26, 9005–9011; (e) F. Holtrop, A. R. Jupp, B. J. Kooij, N. P. van Leest, B. de Bruin and J. C. Slootweg, Single-Electron Transfer in Frustrated Lewis Pair Chemistry, *Angew. Chem., Int. Ed.*, 2020, 59, 22210–22216; (f) W. E. Piers, A. J. V. Marwitz and L. G. Mercier, Mechanistic Aspects of Bond Activation with Perfluoroarylboranes, *Inorg. Chem.*, 2011, 50, 12252–12262.
- 14 (a) A. Merschel, D. Rottschäfer, B. Neumann, H.-G. Stammler, M. Ringenberg, M. van Gastel, T. I. Demirer, D. M. Andrada and R. S. Ghadwal, Crystalline Anions Based on Classical N-Heterocyclic Carbenes, *Angew. Chem., Int. Ed.*, 2023, 62, e202215244; (b) J. Fan, A.-P. Koh, J. Zhou, Z.-F. Zhang, C.-S. Wu, R. D. Webster, M.-D. Su and C.-W. So, Tetrakis(N-heterocyclic Carbene)-Diboron(0): Double Single-Electron-Transfer Reactivity, *J. Am. Chem. Soc.*, 2023, 145, 11669–11677; (c) S. Choe, H. Song, H. Choi, S. Yoo, J. Kim, Y. H. Ko and E. Lee, Formation of Highly Stable 1,2-Dicarbonyl Organic Radicals from Cyclic (Alkyl)(amino) carbenes, *Org. Lett.*, 2023, 25, 4292–4297; (d) J. L. Peltier, M. R. Serrato, V. Thery, J. Pecaut, E. Tomás-Mendivil, G. Bertrand, R. Jazzar and D. Martin, An air-stable radical with a redox-chameleonic amide, *Chem. Commun.*, 2023, 59, 595–598; (e) K. Breitwieser, H. Bahmann, R. Weiss and D. Munz, Gauging Radical Stabilization with Carbenes, *Angew. Chem.*, 2022, 134, e202206390; (f) M. M. Hansmann, M. Melaimi and G. Bertrand, Crystalline Monomeric Allenyl/Propargyl Radical, *J. Am. Chem. Soc.*, 2017, 139, 15620–15623; (g) J. K. Mahoney, D. Martin, F. Thomas, C. E. Moore, A. L. Rheingold and G. Bertrand, Air-Persistent Monomeric (Amino)(carboxy) Radicals Derived from Cyclic (Alkyl)(Amino) Carbenes, *J. Am. Chem. Soc.*, 2015, 137, 7519–7525; (h) N. M. Gallagher, H.-Z. Ye, S. Feng, J. Lopez, Y. G. Zhu, T. Van Voorhis, Y. Shao-Horn and J. A. Johnson, An N-Heterocyclic-Carbene-Derived Distonic Radical Cation, *Angew. Chem., Int. Ed.*, 2020, 59, 3952–3955.
- 15 L. E. Lieske, L. A. Freeman, G. Wang, D. A. Dickie, R. J. Gilliard Jr and C. W. Machan, Metal-Free Electrochemical Reduction of Carbon Dioxide Mediated by Cyclic(Alkyl)(Amino) Carbenes, *Chem. – Eur. J.*, 2019, 25, 6098–6101.
- 16 L. A. Freeman, A. D. Obi, H. R. Machost, A. Molino, A. W. Nichols, D. A. Dickie, D. J. D. Wilson, C. W. Machan and R. J. Gilliard, Soluble, crystalline, and thermally stable alkali CO₂⁻ and carbonite (CO₂²⁻) clusters supported by cyclic(alkyl)(amino) carbenes, *Chem. Sci.*, 2021, 12, 3544–3550.
- 17 (a) D. M. Denning, M. D. Thum and D. E. Falvey, Photochemical Reduction of CO₂ Using 1,3-Dimethylimidazolyliene, *Org. Lett.*, 2015, 17, 4152–4155; (b) O. R. Luca, C. C. L. McCrory, N. F. Dalleska and C. A. Koval, The Selective Electrochemical Conversion of Preactivated CO₂ to Methane, *J. Electrochem. Soc.*, 2015, 162, H473–H476.
- 18 (a) E. Theuergarten, T. Bannenberg, M. D. Walter, D. Holschumacher, M. Freytag, C. G. Daniliuc, P. G. Jones and M. Tamm, Computational and experimental investigations of CO₂ and N₂O fixation by sterically demanding N-heterocyclic carbenes (NHC) and NHC/borane FLP systems, *Dalton Trans.*, 2014, 43, 1651–1662; (b) E. L. Kolychev, T. Bannenberg, M. Freytag, C. G. Daniliuc, P. G. Jones and M. Tamm, Reactivity of a Frustrated Lewis Pair and Small-Molecule Activation by an Isolable Arduengo Carbene-B{3,5-(CF₃)₂C₆H₃}₃ Complex, *Chem. – Eur. J.*, 2012, 18, 16938–16946.
- 19 **1c** was generated *in situ* by applying 1 atm of CO₂ to IAd, before adding (BC₆F₅)₃.
- 20 (a) B. J. Knurr and J. M. Weber, Infrared Spectra and Structures of Anionic Complexes of Cobalt with Carbon Dioxide Ligands, *J. Phys. Chem. A*, 2014, 118, 4056–4062; (b) G. Herzberg, *Molecular spectra and molecular structure*, R. E. Krieger Publishing Co., Malabar, FL, Malabar, Fla, 1991, vol. III, p. 598.
- 21 B. R. Van Ausdall, J. L. Glass, K. M. Wiggins, A. M. Aarif and J. Louie, A Systematic Investigation of Factors Influencing the Decarboxylation of Imidazolium Carboxylates, *J. Org. Chem.*, 2009, 74, 7935–7942.
- 22 O. Back, M. Henry-Ellinger, C. D. Martin, D. Martin and G. Bertrand, ³¹P NMR Chemical Shifts of Carbene-Phosphinidene Adducts as an Indicator of the π-Accepting Properties of Carbenes, *Angew. Chem., Int. Ed.*, 2013, 52, 2939–2943.
- 23 IboView – program for analysing molecular electronic structure, based on Intrinsic Atomic Orbitals (IAOs). <http://www.iboview.org>, G. Knizia, *J. Chem. Theory Comput.*, 2013, 9, 4834–4843.

